Geochemistry, Geophysics, Geosystems®

RESEARCH ARTICLE
10.1029/2024GC012084

Lava Lake Spattering Drives Seismic Tremor During the Geldingadalir 2021 Eruption, Iceland

Alea Joachim[1], Eva P. S. Eibl[1], Daniel Müller[2], Thomas R. Walter[1,2], Tom Winder[3], and Nicholas Rawlinson[4]

[1]University of Potsdam, Institute of Geosciences, Potsdam-Golm, Germany, [2]GFZ Helmholtz Centre for Geosciences, Potsdam, Germany, [3]University of Iceland, Reykjavik, Iceland, [4]University of Cambridge, Cambridge, UK

Key Points:

- The 2021 Geldingadalir eruption formed a lava lake in the crater; its lake surface rose slowly and dropped quickly during effusion episodes
- As the lake level dropped, the size of the vigorously boiling area reached a maximum simultaneously with the peak of seismic tremor
- This study sheds light on the generation of the tremor, which is likely caused by surface processes such as bubble bursting or spattering

Supporting Information:

Supporting Information may be found in the online version of this article.

Correspondence to:

A. Joachim,
alea.joachim@uni-potsdam.de

Citation:

Joachim, A., Eibl, E. P. S., Müller, D., Walter, T. R., Winder, T., & Rawlinson, N. (2025). Lava lake spattering drives seismic tremor during the Geldingadalir 2021 eruption, Iceland. *Geochemistry, Geophysics, Geosystems*, *26*, e2024GC012084. https://doi.org/10.1029/2024GC012084

Received 10 FEB 2025
Accepted 22 JUN 2025

Author Contributions:

Conceptualization: Alea Joachim, Eva P. S. Eibl, Daniel Müller, Thomas R. Walter
Data curation: Tom Winder
Formal analysis: Alea Joachim
Funding acquisition: Eva P. S. Eibl, Thomas R. Walter, Nicholas Rawlinson
Investigation: Alea Joachim, Eva P. S. Eibl, Daniel Müller, Thomas R. Walter, Tom Winder, Nicholas Rawlinson

Abstract Volcanic eruptions generate a continuous ground motion that is commonly referred to as tremor. Although tremor is used worldwide for real-time monitoring of volcanoes, the mechanisms involved are generally poorly understood. Here, we study the episodic effusion during 2021 Geldingadalir eruption. We use photogrammetric data and videos acquired by drones hovering over the active lava lake on 8 June 2021, and compare them with volcanic tremor recorded by a seismometer at 1.8 km distance from the vent. This allows us to investigate the timing of tremor, eruption, and the rise and falls of the lava lake. We observe an episodic seismic tremor lasting about 5 min, followed by over 7-min-long repose times. A closer study of one effusion episode reveals that within these 12 min the lava lake rises and falls by 24.6 ± 0.6 m. The rise time is about 10 min, while the lake level drops within 2 min, contrasting with the tremor observations. By combining tremor and video analysis, we show that the tremor amplitude is not related to the lake level, but peaks when the bubble bursting and spattering in the lava lake is at its maximum. We therefore suggest that the tremor is closely related to the bubble bursting activity and is thus indicative of near-surface processes during an eruption. This study provides insights into tremor generation associated with the Geldingadalir eruption, leading to a conceptual model to assess its implications for the characterization and interpretation of dynamic lava lake evolution.

Plain Language Summary When a volcano erupts, the ground vibrates continuously. This long-lasting vibration is called volcanic tremor. However, scientists do not always know what causes it. In this study, we analysed data from the 2021 Geldingadalir eruption, Iceland. We used a drone to take videos of the lava lake and a seismometer to measure the ground vibration. We find that the lava lake in the crater repeatedly rises and falls. The lava lake rises in about 10 min and then drops quickly. The tremor lasts about 5 min and then stops for 7 min. We noticed that the tremor was strongest while the lava lake dropped, and the bursting bubbles were largest. We suggest that the bursting bubbles cause the tremor.

1. Introduction

The Reykjanes Peninsula is the onshore extension of the Reykjanes Ridge, which is a part of the spreading Mid-Atlantic plate boundary. At this boundary, the North American and Eurasian plates spread obliquely to the main spreading direction at a rate of ~18–19 mm/year (DeMets et al., 1994; Einarsson et al., 2023; Sigmundsson et al., 2020), which leads to high volcanic activity and intense seismicity (Einarsson et al., 2023). Along the plate boundary, various structural features can be found such as eruptive fissures, open fissures and normal faults. Clusters of these features, along with a high-temperature geothermal field, define a volcanic system (Einarsson et al., 2023). Overall, four to five (Sæmundsson & Einarsson, 2014) or six (Sæmundsson et al., 2020) volcanic system, trending SE to NW in an en echelon arrangement, are located on the Reykjanes Peninsula and are from east to west: Hengill, Brennisteinsfjöll, Krýsuvík, Fagradalsfjall, Svartsengi, and Reykjanes volcanic systems (Sæmundsson & Einarsson, 2014).

Despite the absence of a high-temperature geothermal field and a fissure swarm, the Fagradalsfjall volcanic system is recognized as a distinct volcanic system (Pedersen et al., 2022b; Sæmundsson et al., 2020) in an embryonic stage (Sæmundsson et al., 2020). The volcanic systems on the Reykjanes Peninsula have exhibited a periodic pattern of activity for thousands of years, with eruptive episodes lasting ~400–500 years at intervals of 800–1,000 years (Sæmundsson et al., 2020). Furthermore, only one volcanic system is active at a time with jumps at intervals of 100–200 years from east to west (Sæmundsson et al., 2020). The Fagradalsfjall volcanic system is the least active volcanic system with the last eruption occurring over 6,000 years ago (Barsotti et al., 2023; Sæmundsson et al., 2020). However, the most recent eruption on the Reykjanes Peninsula occurred 781 years

Methodology: Alea Joachim, Eva P. S. Eibl, Daniel Müller, Thomas R. Walter
Resources: Thomas R. Walter, Nicholas Rawlinson
Software: Alea Joachim
Supervision: Eva P. S. Eibl, Thomas R. Walter
Validation: Alea Joachim, Thomas R. Walter
Visualization: Alea Joachim
Writing – original draft: Alea Joachim
Writing – review & editing: Alea Joachim, Eva P. S. Eibl, Daniel Müller, Thomas R. Walter, Tom Winder, Nicholas Rawlinson

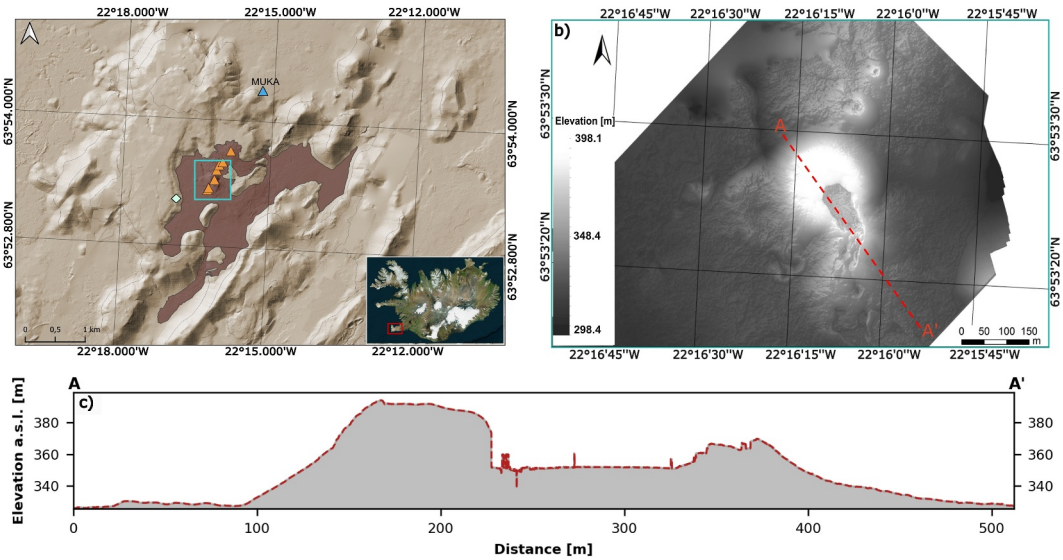

Figure 1. Overview of the eruption site in 2021. (a) Overview map of the eruption site with the extent of the lava flow field, the vents, and a background digital elevation model (DEM) of Geldingadalir valley on 11 June 2021 from Pedersen et al. (2022a). The mint colored square marks the drone launch position, and the cyan rectangle highlights the location of the crater area in (b). (b) The DEM on 8 June 2021 of the active crater featuring a profile line from NW (A) to SE (A′). (c) Profile corresponding to the red dashed line in (b).

prior to the 2021 eruption at Geldingadalir—consistent with the historic periodicity of eruption on the peninsula—and mark the start of a new and potentially long-lived eruption episode (Bindeman et al., 2022; Caracciolo et al., 2023).

The eruption started on 19 March 2021 at about 20:30 UTC next to Mt. Fagradalsfjall (Figure 1a) and ended after 6 months on 18 September 2021 (Barsotti et al., 2023; Pedersen et al., 2022b). More than a year before the onset of the eruption, in mid-December 2019, increased seismicity was observed for several weeks in the vicinity of Mt. Fagradalsfjall (Sigmundsson et al., 2022). The seismic crisis continued in January 2020 at the Svartsengi volcanic system, located west of Fagradalsfjall, and episodes of inflation and deflation have also been observed by GNSS stations and InSAR satellite imagery nearby in the Svartsengi geothermal field (Flóvenz et al., 2022; Geirsson et al., 2021). Overall, three cycles of uplift and subsidence occurred in 2020 in the Reykjanes and Krýsuvík volcanic systems, indicating dyke intrusions (Cubuk-Sabuncu et al., 2021; Geirsson et al., 2021) or hydrothermal activity (Flóvenz et al., 2022). On 24 February 2021, a month before the eruption started, an intense earthquake swarm began in Geldingadalir valley, with around 39,500 earthquakes, the largest of which had a magnitude of Mw 5.6 (Ducrocq et al., 2024; Flóvenz et al., 2022; Sigmundsson et al., 2022). This seismic unrest was interpreted to be the result of an intrusion of a nine-km long dyke between Fagradalsfjall and Keilir, above which a 180-m-long fissure opened on 19 March (Eibl et al., 2023; Sigmundsson et al., 2022).

At the beginning of the eruption, the activity localized at two vents showing steady-bubble bursting, some fountaining activity, and continuous lava outflow (Bindeman et al., 2022; Eibl et al., 2023; Pedersen et al., 2022b). From 5 to 13 April, new vents opened northeast of the original vents (Eibl et al., 2023; Pedersen et al., 2022b). At the end of April, one vent remained the only active vent until the end of the eruption. Before 2 May, it was characterized by continuous lava outflow, and after 2 May, it transitioned into an episodic lava fountaining of varying periodicity and intensity (Eibl et al., 2023; Pedersen et al., 2022b). From May to mid-July, most episodes and reposes were of the order of minutes long but changed to an order of days long from July to September (Eibl et al., 2024).

From the start of the volcanic tremor at 20:30 UTC on 19 March to 1 May 2021, the tremor was continuous (Eibl et al., 2023; Zali et al., 2024). From 2 May 2021, the tremor exhibited an episodic behavior with a distinct start and stop pattern, which was closely linked to the effusion at the active crater (Eibl et al., 2023). A total of 8,698 of these tremor episodes were recorded (Eibl et al., 2024).

Using geophysical monitoring techniques such as seismometers and microphones allow the study of the continuous signal referred to as seismic or acoustic tremor, respectively. Tremor is often emergent and persists for minutes to days, months or years (Acocella, 2021; Cannata et al., 2010; Eibl et al., 2024; Sigurdsson et al., 2015). Tremor is a common observation at volcanoes, where it can occur prior to, during or after eruptions (McNutt & Roman, 2015). In this context, tremor is often known as volcanic tremor. Dominant frequencies of volcanic tremor range from 0.5 to 10 Hz (McNutt & Nishimura, 2008) but have also been observed at frequencies up to 22 Hz at Stromboli volcano (Ripepe et al., 2009) and up to 25 Hz at Ol Doinyo Lengai (Reiss et al., 2023). Tremor often appears continuous but can sometimes also exhibit an episodic behavior.

Several different processes can generate tremor, including surface processes like fountaining activity or ash plumes (Alparone et al., 2003; Eibl et al., 2023; Gottschämmer, 1999; Koyanagi et al., 1987). Subsurface processes, in turn, include bubble coalescence/growth as observed at Erta Ale (Jones et al., 2006), flow-induced oscillations as observed theoretically in modeling studies (Balmforth et al., 2005; Julian, 1994), or hydrothermal boiling of shallow aquifers as observed at Mt. Etna (Cannata et al., 2010). Tremor is also a common observation at lava lakes and is often associated with their activity and fluctuations in level. High seismic amplitudes at Erta Ale lava lake were closely linked to vigorous convection and fountaining activities (Harris et al., 2005), while Richardson et al. (2014) attributed elevated tremor to the bursting of large gas slugs at the surface. At lava lakes like Kīlauea, or Nyiragongo, high tremor amplitudes coincide with vigorous activity, including spattering and outgassing during lava lake fluctuations. These observations suggest that the seismic tremor is likely generated by shallow sources near or at the surface (Barrière et al., 2019; Patrick, Orr, et al., 2011; Patrick, Orr, Swanson, & Lev, 2016).

Active lava lakes form through sustained lava accumulation above vent systems and remain exposed at the surface. In contrast, passive lava lakes or ponds develop in topographic depressions distal to the primary vent (Lev et al., 2019; Tazieff, 1994). Both types are typically associated with open-vent volcanoes and can vary in size, temperature, and depth (Lev et al., 2019; Tazieff, 1994; Witham et al., 2006). They offer a rare but valuable window into subsurface magmatic processes and conduit dynamics' including magma composition, gas release and heat transfer. Currently, six long-term active lava lakes are widely recognized, including Kīlauea volcano (Hawai'i), Erta' Ale volcano (Ethiopia), Nyamuragira volcano and Nyiragongo volcano (D. R. of Congo), Mt. Erebus (Antarctica), and Villarrica volcano (Chile) (Campion & Coppola, 2023; Lev et al., 2019).

Some lava lakes exhibit short- or long-period fluctuations in their level, partly accompanied by changes in their activity from weak to high activity, including spattering, extreme degassing, bubbles bursting, and fountaining (Barrière et al., 2019; Lev et al., 2019; Patrick, Orr, Sutton, et al., 2016; Swanson et al., 1979). On occasion, the level fluctuations exhibit a cyclic behavior comprising a rise followed by a rapid drop, with durations varying. For example, a cycle can last from minutes up to several days for different vertical changes in lake level (Burgi et al., 2014; Patrick, Orr, Sutton, et al., 2016; Patrick, Wilson, et al., 2011; Smets et al., 2017; Swanson et al., 1979). This phenomenon, commonly referred to as gas-pistoning, has been observed several times at lava lakes (Barker et al., 2003; Patrick, Wilson, et al., 2011; Smets et al., 2017; Swanson et al., 1979). It provides insights into conduit processes and the general dynamics of magmatic systems beneath volcanoes (Patrick, Orr, Sutton, et al., 2016; Valade et al., 2018; Witham et al., 2006).

Here, we jointly investigate volcanic tremor recorded using a seismometer and high-quality drone video recordings on 8 June during the 2021 Geldingadalir eruption. Lava lake levels, the vigorous boiling activity of the lava lake and the drone footage we collected in Iceland are all analyzed for the first time in this study. Thus, they provide exceptional insights into the open-vent system of this eruption and may yield new constraints on lava lakes and tremor generation processes. We describe the geometry of the crater (Section 3.1) and assess the lava lake level over time and other parameters such as the overflow timings (Section 3.2), the volcanic tremor (Section 3.3) and the diameter of the vigorously boiling area (Section 3.4) for comparison. Later, we discuss limitations (Section 4.1), compare this lava lake to other lava lakes (Section 4.2), compare the mechanism of the lake behavior (Section 4.3), and discuss a possible link between the tremor and the lava lake (Section 4.4). Finally, we discuss possible sources that may generate the tremor (Section 4.5).

2. Data and Methodology

In the field we recorded both the episodic tremor and the level, overflow and activity of the lava lake. We explore video data from drones recording the eruptive cycles of the lava lake, and a broadband seismic station for the tremor analysis, as detailed in the following.

2.1. Image and Video Data Analysis

To analyze the episodes on 8 June 2021, we used high-quality videos and photos recorded by DJI Phantom 4 Pro and DJI Mavic Air 2 drone quadcopters hovering over the eruption vent. The Phantom 4 Pro is equipped with a gimbal stabilized 20 MP camera and a 1 inch CMOS sensor allowing for the acquisition of geotagged 5,472 × 3,078 pixel aerial photographs in nadir view. The Phantom 4 Pro was flown manually at an altitude of ∼120 m and yielded an overlap of 60–70% between the images, which are later used for the photogrammetric processing. The camera positions and resulting point density are higher in the vicinity of the crater than in peripheral areas. The Mavic Air 2 drone has a $\frac{1}{2}$ inch CMOS camera sensor allowing the acquisition in 4K (3840 × 2160 pixels). Both drones were remotely operated from a launch pad at ∼0.8 km distance from the vent (Figure 1a).

We have orchestrated the missions so that (a) the Phantom 4 Pro drone took overlapping photos for photogrammetric reconstruction of the orthomap and a digital elevation model (DEM) using the structure-from-motion (SFM) approach (Westoby et al., 2012) as implemented in Agisoft Metashape 1.6 (Agisoft LLC, 2020) and (b) the Mavic drone took videos recording the rise and the fall of the lava lake as the drone hovered approximately 50–100 m above the crater. We recorded a total of 947 photos and 18 videos between 17:00 and 20:00 UTC on 8 June 2021. The geometry of the crater was constrained from high-resolution drone photogrammetric data, from which we derived a ∼3 cm/pix resolution DEM and orthomosaic. Despite the video data gaps, we could cover five episodes of lava lake rise and fall. We analyzed each episode by focusing on the eruptive behavior and specified several key parameters such as lava lake level and the diameter of the area where large bubbles burst at the lava surface (referred to as the "boiling area").

We define the **overflow period** as the time period when lava flows over the crater rim(s) during heightened activity in the lake. The onset of overflow begins as soon as the lava flows over the rim, whereas the cessation of overflow occurs once no lava flows over the rim. We picked the timings of onset and cessation of the overflows from the drone videos.

To estimate the **lake** level, we defined reference points, for example, recognizable features such as pointed rocks in the crater, which are visible both in the video and also in the computed orthomosaic. These selected reference points were assumed to be stable and did not change during all the 5 considered episodes. Each point in the crater is assigned to a latitude, longitude and elevation value. This way, we also derived a pixel to meter conversion for the video data. Thus, we estimated lake levels relative to the elevations of the reference points. Due to a change in camera position and drone movement, the estimated lava levels depend more on the visibility of defined reference points instead of being measured in a specific time intervals (see Section 4.1).

The lava lake inside the crater is characterized by high activity, including vigorously bubbling lava. The appearance of the lava lake changes with temperature (Witter & Harris, 2007) in our data set from dark gray to red to orange-to-red and bright yellow. We therefore measured the **diameter of the vigorously boiling area** based on red channel values along a profile through the crater. We used the final video recordings (from 19:37:40 to 19:42:20) for this because the drone was in a stable position with little shaking and the camera position remained stable with a direct view into the crater. We extracted a frame every 5 s during the time period and import these frames into the software Fiji ImageJ (Rasband, 2012). We made an exception for the first image and the second image because the lava lake surface does not show large changes in the first 2 min of the episode. Therefore, we extracted the next frame 2 min later and in the end we used 34 frames for the estimation.

To get information about the red channel values that represent the area of the high activity, we split the frames into the single color channels and analyzed only the red channel because it displays a high level of red-orange-yellow colors in the crater. We tried several approaches to derive these values, also checking the green and the blue color channel, and find that using only the red channel gives reliable results for estimating the diameter. We used 8- bit red channel value images. To determine the red channel values, we draw a line across the lake so that the red

channel values for each pixel along this line can be determined as a function of distance. In our case this line was oriented from northwest to southeast. The brighter the pixel, the higher the red channel value, which lies between 0 and 255. We estimated the diameter based on stable red channel values that is a plateau along the profile in the range 200–255. We defined the end point of this plateau where the gray value drops below 200. We tried different thresholds as well, but they did not modify our findings.

2.2. Seismic Data and Processing

To analyze the tremor, we use seismic data from the closest available station to determine when the tremor starts and ends to enable comparison with the lava lake level. Unlike studies of Eibl et al. (2023, 2024), we did not use the data from the seismometer (NUPH) that was installed in June 2021 at a distance of 5.5 km and was negatively affected by wind noise because it was not buried. Instead, we analyze seismic data from the station MUKA, which is a Güralp 6TD broadband seismometer with a corner frequency of 30 s that was located approximately 1.8 km NNE of the active vent (Figure 1a) and sampled the data at a frequency of 100 Hz (Greenfield et al., 2020). It was buried and aligned toward grid-north close to Meradalahnúkar. We analyze the data of 8 June 2021 from 17:00 to 20:00, which aligns with the time period of the videos. The seismic data were trimmed, detrended and tapered with a cosine taper. We also corrected the instrument response to velocity and applied a zero phase, band-pass filter with two corners from 1 to 20 Hz to avoid microseisms. In addition, we calculate the root mean square (RMS) amplitude for a moving window of 10 s and 50% overlap since this still provides good resolution of the temporal changes in the tremor amplitude. We also tested different window lengths, and they do not change the results.

In addition, we specify the start and end of each tremor episode. We use the RMS amplitude data, with a different moving window of 1 s for picking within the same frequency band, jointly with the filtered seismic data. The markers were created using the Pyrocko software Snuffler (Heimann et al., 2017). Based on the tremor markers, we calculate the duration and repose time of the tremor episodes. The **repose time** is defined as the difference between the end of one tremor episode to the start of another tremor episode. We also use the data to derive information about the seismic tremor amplitude, duration and frequency content. Here, we mainly focus on characterizing the prominent tremor signal observed in relation to the cyclic lava lake activity.

3. Results

3.1. Crater Morphology

Photogrammetric data collected on 8 June 2021 show the active crater and three smaller craters aligned from NW to SE (Figure 1b). The active crater features a low lava lake level which is needed for later measurements of height variations. It achieved the highest elevation at ∼ 397 m above sea level and the crater area covers an area of ∼ 6×10^5 m^2. Southwest of the only active crater, the edifices of the first active vents are visible at a low elevation of around 330 m a.s.l., although they are submerged by lava because they still exhibit a higher elevation than the surrounding lava (Figure 1b). The vents northeast of the active crater exhibit lower elevations than the active crater itself ranging from 352 to 363 m above sea level. The active crater has a nearly circular shape, which becomes more elongated and narrower toward the south. In the north, the crater exhibits an overhanging "spatter" roof above part of the lava lake, which collapsed 2 days later on 10 June (Eibl et al., 2023). The lava lake is situated at an elevation of around 350–352 m a.s.l. (Figure 1c) and occupies an area of ∼5,338 m^2 prior to overflow. In contrast, the rim at the southern end is not of uniform shape and comprises several blocks, which reach a height of ∼372 m above sea level; it is from here that the lava flowed out. The rims on both the eastern and western sides of the crater exhibit similar elevations of 380–382 m a.s.l. (Figure 1). However, along the eastern and western outer crater wall and on the "spatter roof", there are some cracks from which gas escaped.

3.2. Cyclic Patterns in the Lava Lake on 8 June 2021

In June 2021, the lava lake exhibited a cyclic behavior of effusion. The start of each cycle is characterized by a quiet lava lake and a flat lava surface, covered by a dark crust. Small bubbles infrequently rise and burst and hence cause a bit of activity on the surface. A few small fluid-filled cracks divide the crust. This initial quiet period persists for a few minutes although the level gradually rises. At a certain point the activity increases, which includes the beginning of lava outflow and the onset of frequently rising bubbles that increase in size. Here, the term **outflow** is defined as lava that flows across the lowest breach in the crater rampart. Additionally, the surface crust breaks into single plates and migrates southward alongside the outflowing direction. As the surface of the

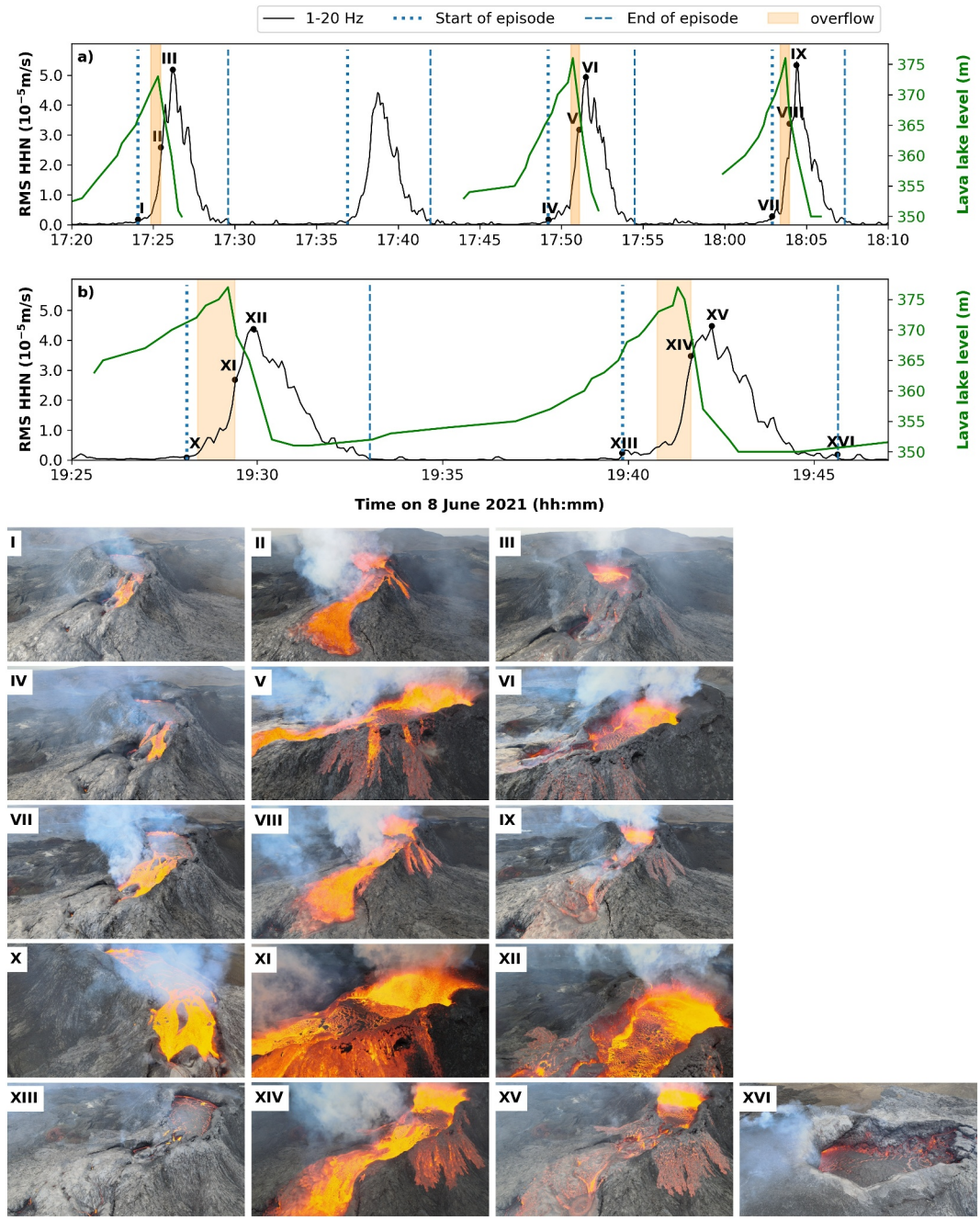

Figure 2. Tremor amplitude compared to lava lake level and overflow periods (a) from 17:20 to 18:10 and (b) 19:25 to 19:46. The green line represents the lava lake level, the black line the RMS of the north component in a frequency band of 1–20 Hz, and the dotted and dashed blue vertical lines represent the start and end of tremor episodes, respectively. We use the north component because it yields the highest amplitude. The overflow is shown by the orange colored area. The Roman numerals mark the timestamps of the images shown below, extracted from the drone footage.

lava lake rises, activity in the lake increases and a larger volume of lava flows out at the lowest breach of the crater rim. More fluid also appears on the surface and splits the crust into smaller plates. At peak lake level, the lava begins to flow over the edge of the higher crater ramparts, which also intensifies the motion in the lake characterized by extreme outgassing, spattering, and bubble bursting.

Each episode exhibits overflows on at least one side of the crater but some also cause overflows on both sides (Figure 2). Furthermore, the lava exhibits higher flow velocities during overflow once the lake reached the spatter

Table 1
Cycle Durations of Tremor and the Lava Lake on 8 June 2021

	Start of tremor	End of tremor	Tremor duration	Repose time	Duration of lake rise	Duration of lake drop
Episode 1	17:24:04	17:29:35	5.52 min	6.57 min	>6.6 min*	1.45 min
Episode 2	17:49:12	17:54:29	5.28 min	8.42 min	>6.67 min*	1.57 min
Episode 3	18:02:54	18:07:20	4.43 min	6.52 min	>3.83 min*	1.57 min
Episode 4	19:28:06	19:33:02	4.93 min	6.8 min	>3.6 min*	1.78 min
Episode 5	19:39:50	19:45:38	5.08 min	7.87 min	10.03 min	1.63 min
Mean	–	–	5.05 min	7.24 min	10.03 min	1.6 min
Standard deviation	–	–	0.37 min	0.77 min	–	0.11 min

Note. The rise duration is calculated from the minimum to the maximum level and the drop duration is calculated from the maximum to the minimum level. The asterisk indicates incomplete durations of the episodes due to missing data as the drone flew back to the base or a change in camera view. The repose time is the one following the tremor.

roof. The original crust is no longer present and instead the surface consists of fluid lava and small plates. Thus, the lava lake level rises slowly within 10.03 min with low surface activity, valid for the most accurate episode. The high lava level remains for a few seconds until the lava surface falls rapidly within 1.63 min to its previous level of 350–352 m above sea level (Figures 2a and 2b). During all cycles, the fluctuations between the lowest and highest level amount to 24.6 ± 0.6 m. The vigorous activity of bubble bursting and spattering remains for another ∼0.83 min when the lake returns to its lowest state, but ceases over time, after which a crust forms on the lava surface. However, spattering stops before the bubble bursting stops and before the latter one stops, a delimited circular area of upwelling forms, which likely marks the location of the conduit. In this area, still larger bubbles burst before activity stops entirely. When activity is no longer visible, a new effusion cycle may begin.

In summary, a cycle is characterized by a slow lava lake level rise with low surface activity and a rapid lake level drop.

On 8 June, the volcanic tremor exhibits a cyclic behavior (black line in Figure 2) (more details on the frequency content in Section 3.3). During the rise of the lava lake the volcanic tremor amplitude is low, but it is higher or at its maximum when the lava lake surface drops (Figure 2). The tremor duration is shorter than the lava lake level rise times (Table 1). However, the lava lake drops within 1.6 ± 0.1 min which is faster than the decrease in tremor amplitude (Figures 2a and 2b). If we compare the highest lava lake level with the maximum tremor amplitude, we observe a temporal offset between them.

Another characteristic of the eruption cycle are the lava overflows, which begin before the tremor onset during each episode. Furthermore, the overflow duration is different between the episodes and ranges from 33 s to 1 min (Figure 2) but they all end before the tremor amplitude reaches its maximum (Figures 2a and 2b).

3.3. Properties of the Volcanic Tremor

On 8 June 2021, the volcanic tremor is characterized by episodic behavior and exhibits high frequency content at least up to 20 Hz (Figure 3). The amplitude is larger on the horizontal components than on the vertical component. However, all tremor episodes exhibit similar amplitudes with slight deviations in their maximum ground velocity. The duration and repose times of each episode are slightly different. The analyzed episodes here exhibit a mean duration of about 5.05 ± 0.37 min (Table 1). In contrast, the repose times are longer with mean durations of about 7.24 ± 0.77 min. Thus, a cycle, consisting of tremor episode and repose time, can last up to 12.28 ± 0.96 min.

3.4. Tremor Amplitude Correlates With the Diameter of the Vigorously Boiling Area

Based on the red channel values, we estimate the diameter of the vigorously boiling area and plot it as function of time (Figures 4b–4e). During the start of the fifth episode the lava surface exhibits a flat and dark surface and thus the diameter is low. At this point in time, the surface along the profile is alternating between crust in form of plates and fluid as described in Section 3.2. The diameter increases with time as the activity on the surface increases (Figures 4c and 4g). At around 19:41:00, the diameter values steadily increase alongside with the activity in the crater (Figure 4d). In total the diameter increases up to ∼30 m before it decreases. This area with increasing

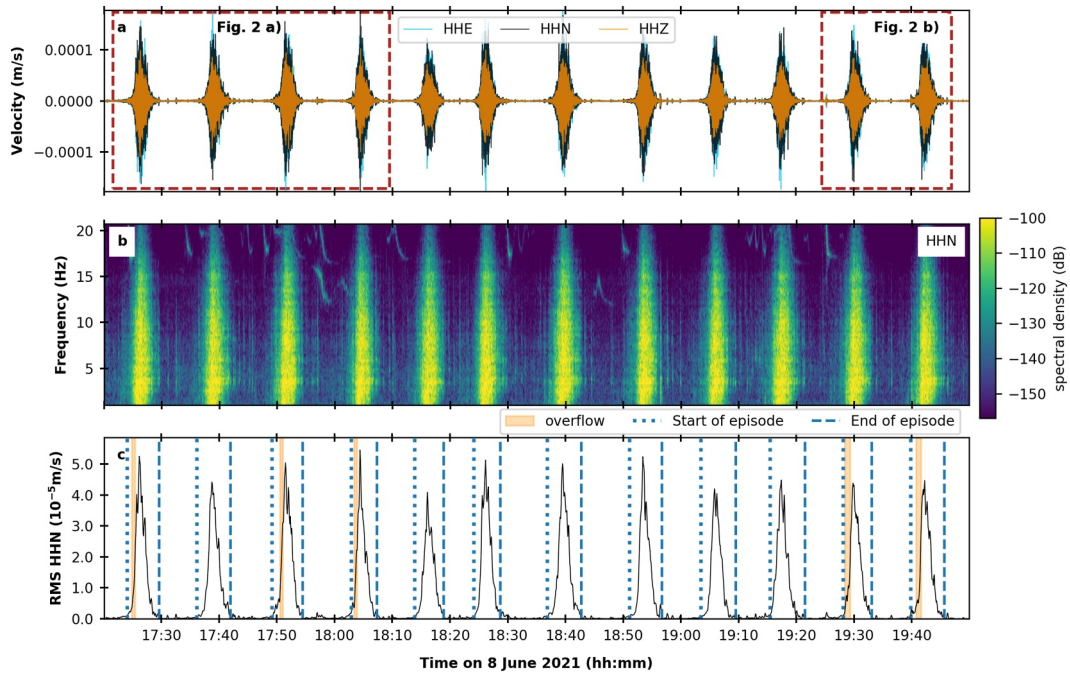

Figure 3. Episodic tremor pattern on 8 June 2021. (a) Seismogram of the East (blue), North (black) and vertical (orange) components, (b) spectrogram showing the spectral amplitude of the North component with a moving time window of 10 s and no overlap, (c) RMS of the North component in a 10 s moving window with overflow times marked. All subfigures are filtered with a band-pass of 1–20 Hz. The dotted vertical lines refer to the start of a tremor episode while the dashed lines represent the end of a tremor episode.

diameter is characterized by surface processes like bubble bursting, spattering, and fountaining (Figures 4h and 4i).

If we compare the lava lake level curve and the tremor amplitude with the diameter of the vigorously boiling area, the tremor amplitude and diameter correlate. Both reach their maximum roughly at the same time with a shift of ∼15 s (Figure 4a). However, the diameter drops earlier but the spattering and bubble bursting remains at high levels (Figure 2 XV). An explanation might be that the diameter is reduced by intense motion caused by the vigorous boiling behavior in the lake and due to the intense motion, a part of the vigorously boiling area is obscured by crust. Furthermore, during the drop of the lava lake, the diameter of the vigorously boiling area still increases in size. However, we could not estimate the diameter at the end of the tremor episode due to a lack of data (Section 4.1). Nonetheless, if we also use the frames in Figure S1 of Supporting Information S1, we expect the diameter to decrease because the vigorously boiling area is smaller compared to the diameter at 19:41:55 (Figure 4). Therefore, the tremor amplitude increases simultaneously with the diameter of the vigorously boiling area, which represents the area of the highest activity (see Figures 4g–4i).

4. Discussion

4.1. Limitations

The combination of drone data and seismic data provides an overview of the volcanic behavior during the Geldingadalir 2021 eruption. We will discuss the limitations of our analysis first.

For the video analysis, it is essential to have the precise timing of the recording for a comparison with other data sets or determine a time stamp for, for example, specific events such as a lava fountain. In this work, we compared drone-derived videos with seismic data, so an accurate time stamp was essential. However, limitations in the synchronization of the video data with the system time of the computer to process the data made it difficult to determine the exact timing. The issue was resolved by checking the flight log files of the quadcopter, which contain the GPS information such as the original time, the location and flight altitude.

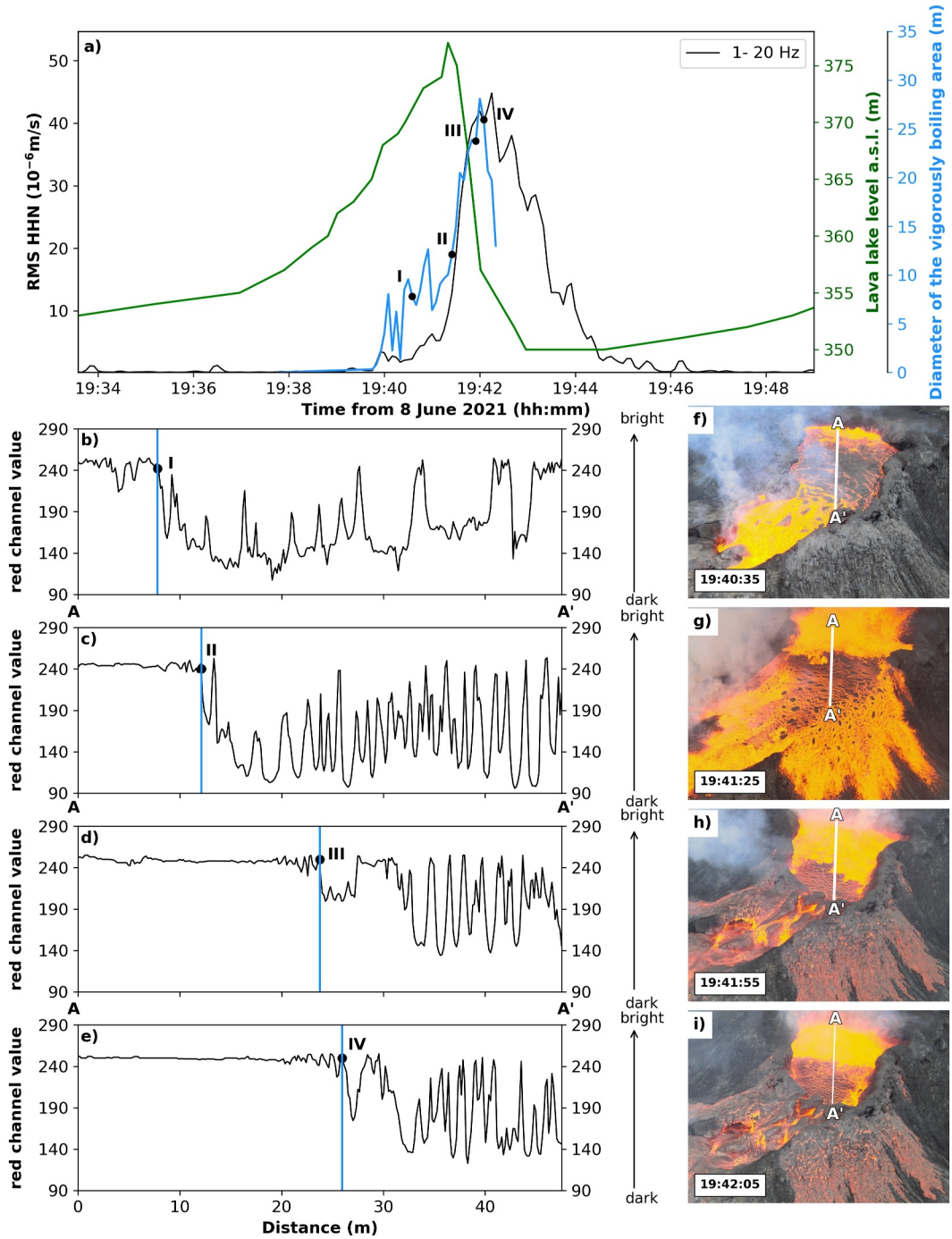

Figure 4. The diameter of the vigorously boiling area correlates with the tremor amplitude. (a) Tremor amplitude in a frequency band of 1–20 Hz (black line), lake level (green line) and the diameter of the vigorously boiling area (blue line). The subfigures (b–e) represent the red channel values of the lake for selected times: (b) 19:40:35, (c) 19:41:25, (d) 19:41:55 and (e) 19:42:05. The Roman numerals correspond to the numbers in (a). The images (f–i) are extracted frames from the videos and correspond to the red channel plots in (b–e).

The drone shook during the video recordings as it hovered above the crater. This also affects the position of the camera, resulting in a slight shift in the field of view. Drones remain in motion, so slight movement or shaking can occur, but stronger movement can be caused by wind. However, the drone's position also changed as it flew around the crater or back to where it started to change batteries. The camera view also changed because of the

movement of the camera itself (e.g., if the camera view was horizontal before it changed to vertical down). These are some of the reasons why there are data gaps. The lava lake levels for several of our analyzed effusion episodes cannot be resolved accurately because of the change in camera view, the large distance to the crater, or the required battery change. In addition, due to the moving drone, the red channel values could only be determined for one episode, since all the others did not have the same field of view for an entire episode. Here we determined the red channel values by taking a profile through the crater which might be slightly shifted due to the drone movement. Small shifts, either horizontally or vertically, may result in small errors because the profile may not be in the identical position in the given extracted frame.

Another factor that affects the video analysis is the gas plume. First, depending on its density, the gas plume obscures the view of the crater, so that parts of the crater are less visible, and levels cannot be accurately estimated. However, the effect of gas plume on visibility and level estimation also depends on the position of the camera on the drone and the viewing angle. In addition, the gas plume also affects our red channel values estimates. The gas plume is bright (i.e., white to light gray) and influences the red channel values of darker material. Depending on the density of the gas plume, the red channel values can considerably increase by up to 25–75. Hence the values, such as those for dark and bright materials, exhibit significant deviations. However, we could not quantify by how much the red channel values were affected in each frame. They do not influence our results because the strong degassing starts with higher activity and the values for crusted areas are around 100 and do not reach our lower limit of the required red channel values of the red color channel to estimate the diameter. Furthermore, we just use those values in the range of 200 and 255, showing stable values and exhibit a plateau-like plot (Figure 4e). Once a value falls below 200, the remaining values are no longer included, even if they rise above the threshold of 200 again.

The video data were also used in conjunction with the 3D model (DEM and orthophoto) to estimate the lava lake level. During the photogrammetric acquisition, the lava lake was rising, which means that the inner part of the crater changed. Because the photos were taken every 2 s and the drone covered a larger area, the crater may have changed between the photos taken at different times, resulting in limited resolution of the crater. This can also lead to minor errors in elevations or incorrectly assigned reference points. Furthermore, the lava lake's activity can become more vigorous, and exhibits a sloshing behavior particularly when the lake overflows and then the lava drains back to the conduit. Thus, it is not easy to obtain accurate lake levels during heightened activity. However, interestingly, this phenomenon has not been discussed in previous studies of lava lakes (Barrière et al., 2019; Patrick et al., 2019; Smets et al., 2017). An explanation might be that we used drone footage which involved camera movement and shaking due to the drone's movement as previously mentioned. Furthermore, lava lakes like Nyiragongo or Kīlauea are larger in diameter (Patrick, Orr, Swanson, & Lev, 2016) and do not exhibit frequent overflows.

Photogrammetric processing depending on the flight parameters or camera system used, may also result in within-model errors and spatial offsets. The Phantom 4 Pro quadcopter during our acquisition uses a single band onboard GPS. Kalacska et al. (2020) stated that using drones with onboard GPS only, without the use of ground control points, can result in lower vertical and horizontal position accuracy with horizontal offsets of ± 5 m and vertical offsets of up to tens of meters. This may result in mean horizontal within-model errors between ∼0.18–0.22 m (Kalacska et al., 2020) and has to be considered for quantification of several measurements.

4.2. Geldingadalir Lava Lake Compared to Nyiragongo and Kīlauea Lava Lakes

During the Geldingadalir eruption, a lava lake formed within an active vent, and featured cyclic fluctuations, including a slowly rising lava surface followed by a rapid drop. Within a 1-hr period, we observe 5 cycles of rises and drops of the lava lake surface. This is evident from the tremor cycles that have a similar cycle duration even though the individual rise and drop period durations are different (Figure 3). Each cycle lasts for less than 12 min, including a slowly rising lake in the first 10 min, followed by a rapid drop on a time scale of less than 2 min. Furthermore, the lake level consistently drops and rises with a total vertical displacement of ∼24.6 m. During each draining event the lake drops to its previous level, although the maximum level exhibits minor fluctuations in level (Figure 2).

Similar observations were made at several open-vent volcanoes that host an active lava lake. These fluctuations or changes in lake level can range from a few meters to tens of meters within a minute or on longer timescales up to several hours, days, or even months (Barrière et al., 2022; Burgi et al., 2014; Patrick et al., 2019). Moreover, lava

level changes are often accompanied by changes in surface processes or activity, such as that observed at Kīlauea or Nyiragongo.

Short-term fluctuations in level have been observed by Swanson et al. (1979) at Mauna Ulu crater with a rise of the lava surface of 30–50 m within 10–15 min or at Pu′u′ ō′ō with changes in level at a similar scale, but with a total cycle duration of minutes to several hours (Barker et al., 2003). In contrast, at some lava lakes the drop in level is often rapid. This was observed at Nyiragongo volcano with a drop of 25 m within a minute in June 2011 or at Kīlauea with 30–50 m in less than 2 min during the activity at the end of July 1969 (Burgi et al., 2014; Swanson et al., 1979).

In contrast to short-term fluctuations, long-term changes have also been observed for example at Kīlauea, where a complete cycle lasted around 1.6–7.8 hr with vertical changes of 11–22 m determined for several events, occurring from November to December 2010 (Patrick, Orr, Sutton, et al., 2016). Interestingly, they observed a cycle that consists of three phases instead of two, including a rapid rise phase, a plateau phase (i.e., lake remains at a high constant level) and a rapid drop phase. Valade et al. (2018) reported a drop and rise of 1.6 m within an hour at the Nyiragongo lava lake in 2016. In contrast, Barrière et al. (2019) observed a rapid 2.5 m drop of the lake surface within 8 min whereas Burgi et al. (2014) observed a rise of a few meters over 4 days in 2010. Here, we could not observe long-term changes due to a limited drone data set with a fixed viewing angle.

Nonetheless, independent of long-term changes at lava lakes, fluctuations are frequently linked to surface processes. Our results indicate similar characteristics as observed at lava lake. During the rise of the lake at Geldingadalir, the surface exhibits a crust, crossed by cracks filled with fluid lava and a few, infrequent bubbles that rise and burst. Several studies about lava lakes mention similar observations such as a crusted surface, weak activity low or passive outgassing during several eruptive phases at Kīlauea (e.g., Mauna Ulu (Swanson et al., 1979) or Halema'uma'u (Patrick, Orr, Sutton, et al., 2016)). A similar observation of weak activity, that is, less degassing and less spattering, was made at Nyiragongo volcano during the rise of the lava surface (Barrière et al., 2019). Occasionally, overflows over the crater can be observed at Nyiragongo when the lake reaches the top of the rampart (Burgi et al., 2014).

In most cases, after the maximum level is reached, the drop is often accompanied by high activity including extreme degassing that is frequently associated with heightened SO_2 values (e.g., at Kīlauea (Patrick, Orr, Sutton, et al., 2016)), spattering and/or bursting of bubbles, and the shattering of the surface crust into plates (Barker et al., 2003; Patrick, Orr, Sutton, et al., 2016; Swanson et al., 1979). These observations were often made before the drop is initiated. However, other studies, particularly those that focus on Nyiragongo, describe vigorous activity and strong degassing after the major draining of the lake, including strong Strombolian activity and meter-sized bubbles that burst (Barrière et al., 2019; Burgi et al., 2014). In case of the 2021 Geldingadalir eruption, before the onset of vigorous activity, we observe outflows of lava and increased flow velocity in the lake. None of the studies about lava lakes observed outflowing coupled with subsequent rising of the magma column. This may be linked to the crater morphology, which is not circular in shape but elongated toward the southwest where the crater rampart elevation is lowest (Figure 1c). This facilitates the outflow of lava. Notwithstanding the outflow of lava, the surface of the lake continues to rise until the overflows commence and the lake drops to its previous level. The lava lake activity increases (i.e., more larger bubbles burst) when the spatter roof of the crater is reached, suggesting that it may be involved in the change in activity. We observe an intensification of lake activity that may be caused by interaction between the lake surface and/or the gas bubbles. As the bubbles rise in the magma column and reach the spatter roof, the bubbles cannot escape and are trapped. However, the lake surface moves (i.e., as observed by way of the crust) along with the bubbles, which are still located above the conduit and can burst. Furthermore interactions with the crater margins seem to affect the surface activity in the lake, similar to what is observed at Kīlauea volcano (Patrick, Orr, Sutton, et al., 2016). The still rising lake and increased activity leads to overflows of the Geldingadalir lake, which was also observed at Nyiragongo volcano caused by the slow rise of the lava surface or the fountaining (Burgi et al., 2014). Here, the vigorous activity, characterized by spattering, bubble bursting, and increased release of gas, is observed before and during the drop of the lake surface. The lake activity remains vigorous but steadily decreases after the return to the starting lake level until only a few smaller bubbles reach the surface and burst.

Our observations of the Geldingadalir lava lake are in accordance with those of persistent lava lakes, especially the main characteristics such as the cyclic behavior and the accompanying changes in activity.

4.3. The Underlying Mechanism for the Cyclic Lake Behavior

Since the lava lake at Geldingadalir exhibits similar characteristics as persistent lava lakes, we suggest that a similar process is at play. Short-lived cycles of lava lake fluctuations, which we observed with durations of up to 8 min, are known as "gas-pistoning" (Barker et al., 2003). Gas-pistoning was observed several times during eruptive phases at Kīlauea (Ferrazzini et al., 1991; Patrick, Wilson, et al., 2011; Swanson et al., 1979, etc.). Each gas-pistoning event commences with the appearance of small bubbles that burst on the lake surface. These bubbles also increase in size and number leading to a heightened gas release (Ferrazzini et al., 1991). As soon as the gas is released, a rapid fall, also known as drainback or draining, is initiated and the lava flows back to the conduit (Ferrazzini et al., 1991). The lake in the shallow part of the crater may have formed due to upward pressure from the accumulated gas, as in the case of Pu′u′ ō′ō crater (Ferrazzini et al., 1991). Some craters drain completely, that is no lava lake remains in the crater, like Pu′u′ ō′ō crater (Barker et al., 2003; Ferrazzini et al., 1991), but the crater in our study still exhibits a lava lake and instead falls to its previous level at an elevation of ∼350 m. A similar observation of fall to the previous lake level after violent activity was made during the Mauna Ulu eruption (Swanson et al., 1979). Nevertheless, as gas-pistoning starts with the appearance of small bubbles, our observations also include the infrequent rise of small bubbles during the slowly upward movement of the lake, which supports the process of gas-pistoning during the Geldingadalir eruption. As these bubbles increase in size, vigorous activity in the lake ensues, including the spattering.

Several explanations have been proposed for the mechanism of gas-pistoning, which are either related to a deeper source (Witham et al., 2006) or a shallow source (Orr & Rea, 2012; Patrick, Orr, Sutton, et al., 2016; Swanson et al., 1979). Witham et al. (2006) proposed that the rising magma is caused by a gas supply from a subsurface reservoir. This reservoir contains degassed magma, with the liberated gas driving the magma up through the conduit and causing the lava lake to rise. On the lake surface, extreme degassing through bubbles or gas slugs might cause an instability in the magma column due to the large amount of released gas. This results in a drop of the lava to the conduit and no further bubbles can ascend until the lake is drained, because they are trapped by the down flowing lava (Witham et al., 2006). Also a similar process was proposed during an active phase at Kīlauea (Barker et al., 2003). The rise of the lava lake is caused by vesiculation in the magma column beneath the vent, leading to an extension of the lava surface at the top, while the abrupt release of gas leads to a drop of the lake similar as described by Witham et al. (2006). Because of the down flowing lava, the magma column closes the conduit and also hinders the escape of gas (Barker et al., 2003). Thus, the gas release is higher during the rising phase than during the falling stage (Witham et al., 2006). In contrast, shallow sources proposed to explain gas-pistoning are thought to be located near the surface or just below the crust, where a gas-rich layer may exist, as suggested by Patrick, Orr, Sutton, et al. (2016). Their observations of passive outgassing during both spattering and non-spattering activity at Kīlauea support the presence of such a layer. Additionally, rockfalls can trigger significant and rapid drops in the lava lake surface by disturbing and collapsing this gas-rich layer, releasing accumulated gas. However, not all rockfalls result in such drops—smaller events may only cause localized spattering. At the same time, gas emissions and seismic amplitudes tend to decrease as the lake rises, indicating an inverse relationship (Patrick, Orr, Sutton, et al., 2016; Patrick, Orr, Swanson, & Lev, 2016). Patrick, Orr, et al. (2011) observed gas-pistoning in a perched lava channel, which can also be explained by a gas accumulation beneath the surface crust. However, Orr and Rea (2012) suggested the presence of a shallow foam layer beneath the encrusted surface based on observations during gas-pistoning in 2006 at Pu′u′ ō′ō cone. Unlike other proposed mechanisms, the foam layer is stable enough to prevent no cracks from forming within the crust during the rise of the lake, which could explain the reduced brightness of the surface. The proposed mechanisms for gas-pistoning, as outlined above, do not entirely accord with our observations. We still observe bubbles bursting and spattering (i.e., release of gas) during and after a decrease in the lava lake level and it does not appear that the gas is trapped by lava flowing back into the conduit. Furthermore, we did not observe any (larger) rockfalls during higher lake levels, but after the draining of the lake, small rockfalls did occur due to an unstable crater roof of fresh lava (Movie S1 at 00:00:21). We cannot completely exclude that larger rockfalls occur and trigger an abrupt drop of this lake, because our video footage only covers five episodes of effusion and not the entire day. Small rockfalls occurring after the drop of the lake cause local and small spatter sources which also suggest a shallow source (Patrick, Orr, Sutton, et al., 2016). Here, it is more likely that the drop in level is caused by the release of gas by large gas bubbles and/or spattering events. While the lake is dropping to its previous level, bubbles still burst and the high boiling activity remains, though it decreases over time. Thus, bubbles can still ascend but might generate sufficient pressure to elevate the surface. Thus, this observation would partly exclude the suggestion of a deeper

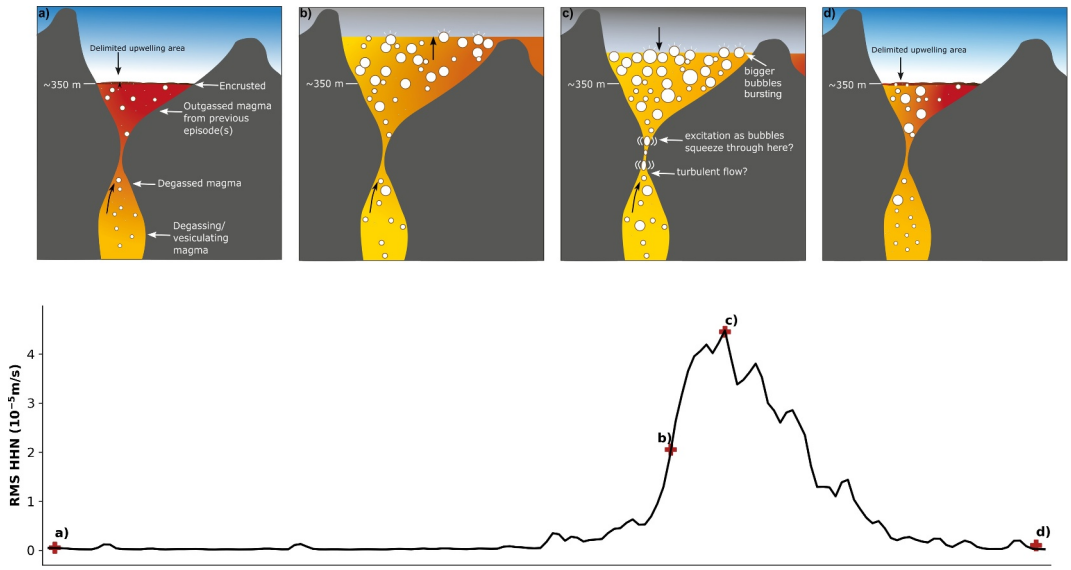

Figure 5. Schematic model of lava lake dynamics with the corresponding tremor amplitude shown as RMS amplitude. The RMS is band-pass filtered between 1 and 20 Hz with a 10 s window length. The phases of the lava lake cycle at Geldingadalir lava lake are illustrated in panels (a–d). The colors in the scheme correspond to the colors of the lava lake surface during the various phases. The letters in the RMS curve refer to the different phases of the scheme.

source proposed by Witham et al. (2006) that upward migration of the bubbles is completely arrested after the lake fall. However, we suggest that the behavior of gas-pistoning at Geldingadalir also involves vesiculation of bubbles (including the ascent of small bubbles through the conduit, which later coalesce to form larger single bubbles or slugs) as suggested by Witham et al. (2006).

We also observe a delimited circular area of upwelling, where larger bubbles burst, after the decrease of the boiling activity and the draining of the lake (see Movie S1 from minute 00:03:50 or Figures 5a and 5d). Previous studies about lava lakes (Barker et al., 2003; Patrick, Orr, Sutton, et al., 2016; Witham et al., 2006) did not describe a delimited upwelling area at the onset of the rise of the lava lake but also identify an upwelling area. Molina et al. (2015) made similar observations at Mt. Erebus and called them "magma batches." In contrast to the Geldingadalir lava lake, they observe several magma batches, which overlaid each other, but they did not observe "gas-pistoning." These magma batches are developed at depth from dissolved gas in ascending magma (Molina et al., 2015). The dissolved gas rises due to buoyancy and exsolves when the pressure decreases. However, the development of a magma batch is not entirely understood yet, but it may be linked to flow instability (Molina et al., 2015). When a magma batch reaches the surface, it causes upwelling on the lava lake surface because it contains an extra supply of bubbly magma, which releases the liberated gas into the atmosphere (Molina et al., 2015). The degassed melt then spreads toward the edges of the lake while degassed and cooled magma is drained back to the conduit (Molina et al., 2015). Such process might explain the existence of larger bubbles before the lake again starts to rise.

The cyclic behavior of the lava lake level at Geldingadalir can be linked to gas-pistoning, and would be the first known gas-pistoning observed during an Icelandic eruption. However, despite the fresh insight brought about by this study, we cannot completely determine the mechanism underlying the gas-pistoning during this eruption since several processes exists that drive this behavior. We would rather consider a shallow process of shallow gas accumulation than a deeper one.

4.4. Link Between Tremor Amplitude and Lava Lake Level

Lava lake fluctuations are a common observation at basaltic open-vent volcanoes and have been studied in detail using a variety of geophysical and geochemical parameters. We studied lava lake fluctuations in terms of volcanic tremor, which we recorded at a nearby seismometer. Volcanic tremor during the Geldingadalir eruption occurs episodically with a duration of ~5.05 ± 0.37 min and 7.24 ± 0.77 min of repose time. Thus, the tremor exhibits a cyclic behavior and occurs approximately five times an hour, which is also the frequency of the lava lake

fluctuations. Similar observations have been made at Kīlauea on several occasions. For example, episodic tremor has been observed at Kīlauea during an eruptive phase in Halema'uma'u crater. The occurrence of episodic tremor started a month after the onset of the eruption and became regular, with episodes occurring every 5–10 min (Patrick et al., 2008; Patrick, Orr, Sutton, et al., 2016). However, Patrick, Wilson, et al. (2011) also observed episodic tremor with a total of five spindle-shaped episodes in an hour on a single day in June 2009. Before and after the occurrence of these episodic tremor, continuous tremor with a lower amplitude was also recorded. During another eruptive phase of Kīlauea in 1999 at Pu′u′ ō′ō crater, Barker et al. (2003) observed reappearing banded tremor. In these studies, the episodic tremor was associated with the cyclic lava lake behavior, characterized by a rise and a fall of the lake surface. The tremor started when an abrupt drainback of the lake surface (i.e., fall of the lake) was initiated and stopped when the surface started to rise (Barker et al., 2003; Nadeau et al., 2015; Patrick, Wilson, et al., 2011). Barker et al. (2003) reported that the tremor did not always start with the onset of fall of the lake, caused by the gas release, but also occurred a few minutes before or after. Tremor was also observed and linked to lake fluctuations at Nyiragongo volcano despite the absence of episodic tremor patterns (Barrière et al., 2019). The signal was low during the rise of the lake surface and increased to a larger amplitude when the lake drops. We made similar observations: During the rise of the lake surface, there is no tremor; instead, it begins several minutes before the drainback of the lake is initiated and even before the overflow occurs. When the lake is dropping, the tremor exhibits a high amplitude and remains high for a few minutes after the drop (Figure 4a). At Kīlauea, a similar observation was made with the tremor remaining high for some 30–45 min after the drainback stopped. In some cases, the tremor started a few minutes before the drainback was initiated (Barker et al., 2003). Although, we made similar observations, we do not see a direct correlation between the lake level and the episodic tremor. Furthermore, the tremor duration does not coincide with the lake rise duration because the latter occurs for a longer time period (Table 1).

4.5. Possible Sources for the Episodic Tremor

In the absence of a direct correlation between the lake level and the episodic tremor, particularly in the context of the draining event observed at lava lakes, we still suggest a regular and cyclic source. Another parameter that manifests in a cyclical manner throughout each episode is the high level of activity, which encompasses the spattering, outgassing and bursting of bubbles. We represent such occurrences by the diameter of the vigorously boiling area. The start of an episode of increased activity (diameter) coincides with the start of the tremor episode, respectively. Additionally, the largest diameter of the vigorously boiling area coincides with a high tremor amplitude, which occurs when the lake is already dropping (Figure 4a). Thus, visual observations support the interpretation that surface processes generate the tremor. The onset of tremor is characterized by lava outflow and increased surface activity including the bursting of small-to middle-sized bubbles. Remarkable also is that at the end of the tremor, small bubbles still rise and burst on the smooth, black lava lake surface (see Movie S1 from minute 00:03:32).

High tremor amplitudes and even episodic tremor at volcanoes hosting an active lava lake are often linked to surface activity and outgassing processes, including bubble bursting or fountaining. Ferrazzini et al. (1991) observed a change from continuous to episodic tremor during the eruptive phase of Kīlauea at Pu′u′ ō′ō crater. The episodic tremor occurred in regular patterns and was linked to regularly occurring gas-piston events. Furthermore, these gas-piston events were accompanied by an increase in the number and size of bubbles, which also correlated with an increasing seismic amplitude (Ferrazzini et al., 1991). The episodic occurrence of tremor at Villarrica was linked to explosive activity with an increase of gas flux and more and larger bubbles bursting and spattering activity (Palma et al., 2008). High frequency signals at Erta Ale volcano, were linked to intense lava lake convection including lava fountaining and a thin crust. When the crust thickened and the convection was slow, this signal was absent or infrequent (Harris et al., 2005). Thus, Harris et al. (2005) also found a link between seismic amplitude and a surface activity. Processes not directly related to the lake surface convection, such as spattering, were also linked to high tremor amplitudes as observed at Kīlauea (Patrick, Orr, Sutton, et al., 2016; Patrick, Orr, Swanson, & Lev, 2016). During lava lake fluctuations, spattering phases were associated with heightened tremor, as shown by spatter area estimates (Patrick, Orr, Swanson, & Lev, 2016). In contrast, non-spattering phases were characterized by the complete absence of tremor. Thus, shallow processes tend to generate higher frequency signals like tremor, often accompanied by extreme outgassing (Nadeau et al., 2015; Patrick, Orr, Swanson, & Lev, 2016). Thus, shallow processes are in favor of higher frequency signals including tremor.

Our observations also reveal a similar correlation between spattering activity and bubble bursting with episodic tremor, although we have neither quantified the number nor the size of the bubbles. However, using the frames from Figures 4f and 4h, we can clearly see an increase in the number and size of bubbles. Both bubble bursting and spattering activity represent vigorously boiling activity, coinciding with a high tremor amplitude. After draining, a residual low-amplitude tremor persists when the surface activity in the lake ceased. Thus, high amplitude tremor is possibly caused by a combination of bubble bursting and spattering, whereas when the tremor starts we observe smaller bubble bursts (Figure 2 XIII). However, other studies find that small bubbles with a diameter of ∼0.5 m were recorded as infrasonic impulses (Ripepe & Gordeev, 1999). Here, the episodic effusion pattern does not just generate acoustic signals (Lamb et al., 2022) but also seismic signals recorded by a seismometer at a distance of 1.8 km.

While surface related processes generate episodic tremor, we also consider regularly occurring processes in the subsurface (e.g., in the conduit). The cyclic lava lake behavior is probably caused by gas-piston events, although tremor might be generated by bubble growth/coalescence or by the interaction of gas and fluid, particularly during the ascent of magma through the conduit (Figure 5c). Thus, also several processes in the subsurface might generate episodic tremor during the effusion episode of this eruption. We observe bigger bursting bubbles on the surface, which were initially small within the shallow magmatic system. When they ascend within the magma column, they coalesce and grow in size. They might be so large that they are squeezed through a confined part of the conduit, leading to tremor due to excitation (Figure 5c). Such subsurface processes can also be considered to generate tremor and have been described in a few studies. A seismic signal caused by magmatic fluid transport, ascending through a narrow conduit, was observed in an experiment (James et al., 2006). However, they did not observe tremor but long-period and very long period signals. While the coalescence of gas bubbles generates seismic tremor and the bursting of these bubbles generates infrasonic pulses at Stromboli (Ripepe & Gordeev, 1999). A similar observation was observed at Erta Ale, where tremor was partly generated by a subsurface source involving bubble coalescence in the conduit itself and in the lava lake (Jones et al., 2006). Also, flow-induced oscillations like turbulent flows in conduits or channels caused by magmatic fluid can generate several tremor characteristics (Julian, 1994). Several models have been tested and suggest that the flow-induced oscillations can cause tremor, especially at volcanoes that erupt through narrow conduits with high fluid velocities. This is called "flow-induced tremor" since magma itself cannot generate flow induced vibrations (Balmforth et al., 2005). However, fluid movement containing gas bubbles with a constant flow velocity cannot generate tremor, only when the ascending gas bubbles within the magma proceeds with high velocities (Ripepe & Gordeev, 1999). Nevertheless, we can exclude high fluid velocities as source for tremor generation because our tremor amplitude is heightened when the lava falls back to the previous level (Figure 5c). Otherwise, we would expect heightened tremor amplitude during the lake rise. We cannot exclude a tremor generation at depth, but as the tremor amplitude is tightly linked to the area with vigorous boiling activity, it seems most likely that tremor is generated by surface activity like bursting bubbles or spattering as also observed several times at Kīlauea (Patrick, Orr, Sutton, et al., 2016; Patrick, Orr, Swanson, & Lev, 2016).

5. Conclusions

The 2021 Geldingadalir eruption featured an active lava lake with a cyclic behavior of lava level rise and drop, which we attribute to gas-pistoning that is observed at lava lakes, elsewhere. This study has revealed for the first time that gas-pistoning can be observed during an Icelandic eruption typically characterized by cyclic lava lake fluctuations. The cyclic behavior, in which a cycle lasts for around 12 min, also shows distinct characteristics such as vigorously boiling activity that includes bursting bubbles and spattering before and during the fall of the lake level, while the rising phase is characterized by a thin crust. Furthermore, the tremor exhibits a cyclic behavior, also of around 12 min duration, with a tremor period and a quiescence period.

We find no direct correlation between lava lake fluctuations and tremor, but we find a link between tremor amplitude and the size of the vigorously boiling area featuring bubble bursting and spattering. It is hence likely that the tremor is generated by the number or size of the bursting bubbles caused by the gas release. However, other models linking tremor to for example, larger flow velocities, bubble coalescence or bubble ascent through a narrow conduit cannot be fully excluded. Additional data sets like acoustic data or gas emissions might be helpful in future studies to better illuminate the episodic tremor generation process. Nevertheless, the use of drone videos in addition to other observational tools, provide exceptional insight into the surface processes of volcanoes.

Data Availability Statement

The seismic data from MUKA are already available on IRIS (Greenfield et al., 2020). The video data, the 3D models, and the marker file of 8 June 2021 are available via the GFZ Data Services (Joachim et al., 2025).

Acknowledgments
We thank Marius Isken and Erica de Paolo for support in the field. We would also like to thank Manuela Kaspar for her help with illustrating the schematic model and Matthias Ohrnberger for discussion. Open Access funding enabled and organized by Projekt DEAL.

References

Acocella, V. (2021). Volcano-tectonic processes. In *Advances in Volcanology*. Springer International Publishing. https://doi.org/10.1007/978-3-030-65968-4.

Agisoft LLC. (2020). Agisoft metashape professional. Retrieved from www.agisoft.com/downloads/installer

Alparone, S., Andronico, D., Lodato, L., & Sgroi, T. (2003). Relationship between tremor and volcanic activity during the southeast crater eruption on Mount Etna in early 2000. *Journal of Geophysical Research*, *108*(B5). https://doi.org/10.1029/2002JB001866

Balmforth, N. J., Craster, R. V., & Rust, A. C. (2005). Instability in flow through elastic conduits and volcanic tremor. *Journal of Fluid Mechanics*, *527*, 353–377. https://doi.org/10.1017/s0022112004002800

Barker, S. R., Sherrod, D. R., Lisowski, M., Heliker, C., & Nakata, J. S. (2003). *Correlation between lava-pond drainback, seismicity, and ground deformation at Pu′u ō′ō* (pp. 53–62). USGS Professional Paper (1676). Retrieved from https://www.researchgate.net/publication/289177729_Correlation_between_lava-pond_drainback_seismicity_and_ground_deformation_at_Pu%27u_%27O%27o

Barrière, J., d'Oreye, N., Oth, A., Theys, N., Mashagiro, N., Subira, J., et al. (2019). Seismicity and outgassing dynamics of Nyiragongo volcano. *Earth and Planetary Science Letters*, *528*, 115821. https://doi.org/10.1016/j.epsl.2019.115821

Barrière, J., d'Oreye, N., Smets, B., Oth, A., Delhaye, L., Subira, J., et al. (2022). Intra–crater eruption dynamics at Nyiragongo (D.R. Congo), 2002–2021. *Journal of Geophysical Research: Solid Earth*, *127*(4), e2021JB023858. https://doi.org/10.1029/2021JB023858

Barsotti, S., Parks, M. M., Pfeffer, M. A., Óladóttir, B. A., Barnie, T., Titos, M. M., et al. (2023). The eruption in Fagradalsfjall (2021, Iceland): How the operational monitoring and the volcanic hazard assessment contributed to its safe access. *Natural Hazards*, *116*(3), 3063–3092. https://doi.org/10.1007/s11069-022-05798-7

Bindeman, I. N., Deegan, F. M., Troll, V. R., Thordarson, T., Höskuldsson, Á., Moreland, W. M., et al. (2022). Diverse mantle components with invariant oxygen isotopes in the 2021 Fagradalsfjall eruption, Iceland. *Nature Communications*, *13*(1), 3737. https://doi.org/10.1038/s41467-022-31348-7

Burgi, P.-Y., Darrah, T. H., Tedesco, D., & Eymold, W. K. (2014). Dynamics of the Mount Nyiragongo lava Lake. *Journal of Geophysical Research: Solid Earth*, *119*(5), 4106–4122. https://doi.org/10.1002/2013JB010895

Campion, R., & Coppola, D. (2023). Classification of lava Lakes based on their heat and SO_2 emission: Implications for their formation and feeding processes. *Frontiers in Earth Science*, *11*. https://doi.org/10.3389/feart.2023.1040199

Cannata, A., Di Grazia, G., Montalto, P., Ferrari, F., Nunnari, G., Patanè, D., & Privitera, E. (2010). New insights into banded tremor from the 2008–2009 Mount Etna eruption. *Journal of Geophysical Research*, *115*(B12). https://doi.org/10.1029/2009JB007120

Caracciolo, A., Bali, E., Halldórsson, S. A., Guðfinnsson, G. H., Kahl, M., Þórðardóttir, I., et al. (2023). Magma plumbing architectures and timescales of magmatic processes during historical magmatism on the Reykjanes Peninsula, Iceland. *Earth and Planetary Science Letters*, *621*, 118378. https://doi.org/10.1016/j.epsl.2023.118378

Cubuk-Sabuncu, Y., Jónsdóttir, K., Caudron, C., Lecocq, T., Parks, M. M., Geirsson, H., & Mordret, A. (2021). Temporal seismic velocity changes during the 2020 rapid inflation at Mt. Þorbjörn–Svartsengi, Iceland, using seismic ambient noise. *Geophysical Research Letters*, *48*(11). https://doi.org/10.1029/2020GL092265

DeMets, C., Gordon, R. G., Argus, D. F., & Stein, S. (1994). Effect of recent revisions to the geomagnetic reversal time scale on estimates of current plate motions. *Geophysical Research Letters*, *21*(20), 2191–2194. https://doi.org/10.1029/94GL02118

Ducrocq, C., Árnadóttir, T., Einarsson, P., Jónsson, S., Drouin, V., Geirsson, H., & Hjartardóttir, Á. R. (2024). Widespread fracture movements during a volcano-tectonic unrest: The Reykjanes Peninsula, Iceland, from 2019–2021 TerraSAR-X interferometry. *Bulletin of Volcanology*, *86*(2), 1–12. https://doi.org/10.1007/s00445-023-01699-0

Eibl, E. P. S., Thordarson, T., Höskuldsson, Á., Gudnason, E. Á., Dietrich, T., Hersir, G. P., & Ágústsdóttir, T. (2023). Evolving shallow conduit revealed by tremor and vent activity observations during episodic lava fountaining of the 2021 Geldingadalir eruption, Iceland. *Bulletin of Volcanology*, *85*(2), 1–20. https://doi.org/10.1007/s00445-022-01622-z

Eibl, E. P. S., Thordarson, T., Moreland, W. M., Gudnason, E. Á., Höskuldsson, Á., Hersir, G. P., & Heimann, S. (2024). Illuminating the transition from an open to a semi–closed Volcanic vent system through episodic tremor duration and shape. *Journal of Geophysical Research: Solid Earth*, *129*(5). https://doi.org/10.1029/2023JB028323

Einarsson, P., Eyjólfsson, V., & Hjartardóttir, Á. R. (2023). Tectonic framework and fault structures in the Fagradalsfjall segment of the Reykjanes Peninsula Oblique rift, Iceland. *Bulletin of Volcanology*, *85*(2), 1–17. https://doi.org/10.1007/s00445-022-01624-x

Ferrazzini, V., Aki, K., & Chouet, B. (1991). Characteristics of seismic waves composing Hawaiian volcanic tremor and gas–piston events observed by a near–source array. *Journal of Geophysical Research*, *96*(B4), 6199–6209. https://doi.org/10.1029/90JB02781

Flóvenz, Ó. G., Wang, R., Hersir, G. P., Dahm, T., Hainzl, S., Vassileva, M., et al. (2022). Cyclical geothermal unrest as a precursor to Iceland's 2021 fagradalsfjall eruption. *Nature Geoscience*, *15*(5), 397–404. https://doi.org/10.1038/s41561-022-00930-5

Geirsson, H., Parks, M., Vogfjörd, K., Einarsson, P., Sigmundsson, F., Jónsdóttir, K., et al. (2021). The 2020 volcano-tectonic unrest at Reykjanes Peninsula, Iceland: Stress triggering and reactivation of several volcanic systems. https://doi.org/10.5194/egusphere-egu21-7534

Gottschämmer, E. (1999). Volcanic tremor associated with eruptive activity at Bromo volcano. *Annals of Geophysics*, *42*(3). https://doi.org/10.4401/ag-3731

Greenfield, T., Rawlinson, N., Winder, T., & Brandsdóttir, B. (2020). Reykjanes seismic network. *International Federation of Digital Seismograph Networks*. https://doi.org/10.7914/SN/8F_2020

Harris, A. J., Carniel, R., & Jones, J. (2005). Identification of variable convective regimes at Erta ale lava Lake. *Journal of Volcanology and Geothermal Research*, *142*(3–4), 207–223. https://doi.org/10.1016/j.jvolgeores.2004.11.011

Heimann, S., Kriegerowski, M., Isken, M., Cesca, S., Daout, S., Grigoli, F., et al. (2017). Pyrocko—An open-source seismology toolbox and library. *GFZ Data Services*. https://doi.org/10.5880/GFZ.2.1.2017.001

James, M. R., Lane, S. J., & Chouet, B. A. (2006). Gas slug ascent through changes in conduit diameter: Laboratory insights into a volcano–seismic source process in low–viscosity magmas. *Journal of Geophysical Research*, *111*(B5). https://doi.org/10.1029/2005JB003718

Joachim, A., Eibl, E. P. S., Müller, D., Isken, M. P., de Paolo, E., Walter, T. R., et al. (2025). Drone photos and videos, DEM and orthophoto, marker file of tremor episodes of one day during the 2021 Geldingadalir eruption. *GFZ Data Services*. https://doi.org/10.5880/fidgeo.2025.005

Jones, J., Carniel, R., Harris, A. J., & Malone, S. (2006). Seismic characteristics of variable convection at Erta 'Ale lava Lake, Ethiopia. *Journal of Volcanology and Geothermal Research*, *153*(1–2), 64–79. https://doi.org/10.1016/j.jvolgeores.2005.08.004

Julian, B. R. (1994). Volcanic tremor: Nonlinear excitation by fluid flow. *Journal of Geophysical Research*, *99*(B6), 11859–11877. https://doi.org/10.1029/93JB03129

Kalacska, M., Lucanus, O., Arroyo-Mora, J., Laliberté, É., Elmer, K., Leblanc, G., & Groves, A. (2020). Accuracy of 3D landscape reconstruction without ground control points using different UAS platforms. *Drones*, *4*(2), 13. https://doi.org/10.3390/drones4020013

Koyanagi, R. Y., Chouet, B., & Aki, K. (1987). Origin of volcanic tremor in Hawaii. *U. S. Geological Survey Professional Paper*, *1350*(2), 1221–1257.

Lamb, O. D., Gestrich, J. E., Barnie, T. D., Jónsdóttir, K., Ducrocq, C., Shore, M. J., et al. (2022). Acoustic observations of lava fountain activity during the 2021 Fagradalsfjall eruption, Iceland. *Bulletin of Volcanology*, *84*(11), 1–18. https://doi.org/10.1007/s00445-022-01602-3

Lev, E., Ruprecht, P., Oppenheimer, C., Peters, N., Patrick, M., Hernández, P. A., et al. (2019). A global synthesis of lava Lake dynamics. *Journal of Volcanology and Geothermal Research*, *381*, 16–31. https://doi.org/10.1016/j.jvolgeores.2019.04.010

McNutt, S. R., & Nishimura, T. (2008). Volcanic tremor during eruptions: Temporal characteristics, scaling and constraints on conduit size and processes. *Journal of Volcanology and Geothermal Research*, *178*(1), 10–18. https://doi.org/10.1016/j.jvolgeores.2008.03.010

McNutt, S. R., & Roman, D. C. (2015). Volcanic seismicity. In *The encyclopedia of volcanoes* (pp. 1011–1034). Elsevier Science Publishing Co Inc. https://doi.org/10.1016/b978-0-12-385938-9.00059-6

Molina, I., Burgisser, A., & Oppenheimer, C. (2015). A model of the geochemical and physical fluctuations of the lava Lake at Erebus volcano, Antarctica. *Journal of Volcanology and Geothermal Research*, *308*, 142–157. https://doi.org/10.1016/j.jvolgeores.2015.10.027

Nadeau, P. A., Werner, C. A., Waite, G. P., Carn, S. A., Brewer, I. D., Elias, T., et al. (2015). Using SO_2 camera imagery and seismicity to examine degassing and gas accumulation at Kīlauea Volcano, May 2010. *Journal of Volcanology and Geothermal Research*, *300*, 70–80. https://doi.org/10.1016/j.jvolgeores.2014.12.005

Orr, T. R., & Rea, J. C. (2012). Time-lapse camera observations of gas piston activity at Pu ʻu ʻŌ ʻō, Kīlauea volcano, Hawai ʻi. Bulletin of Volcanology, *74*(10), 2353–2362. https://doi.org/10.1007/s00445-012-0667-0

Palma, J. L., Calder, E. S., Basualto, D., Blake, S., & Rothery, D. A. (2008). Correlations between SO_2 flux, seismicity, and outgassing activity at the open vent of Villarrica volcano, Chile. *Journal of Geophysical Research*, *113*(B10). https://doi.org/10.1029/2008JB005577

Patrick, M., Orr, T., Sutton, A. J., Lev, E., Thelen, W., & Fee, D. (2016a). Shallowly driven fluctuations in lava Lake outgassing (gas pistoning), Kīlauea Volcano. *Earth and Planetary Science Letters*, *433*, 326–338. https://doi.org/10.1016/j.epsl.2015.10.052

Patrick, M., Orr, T., Swanson, D., & Lev, E. (2016b). Shallow and deep controls on lava Lake surface motion at Kīlauea Volcano. *Journal of Volcanology and Geothermal Research*, *328*, 247–261. https://doi.org/10.1016/j.jvolgeores.2016.11.010

Patrick, M., Orr, T., Wilson, D., Dow, D., & Freeman, R. (2011a). Cyclic spattering, seismic tremor, and surface fluctuation within a perched lava channel, Kīlauea Volcano. *Bulletin of Volcanology*, *73*(6), 639–653. https://doi.org/10.1007/s00445-010-0431-2

Patrick, M., Swanson, D., & Orr, T. (2019). A review of controls on lava Lake level: Insights from Halema'uma'u crater, Kīlauea Volcano. *Bulletin of Volcanology*, *81*(3), 13. https://doi.org/10.1007/s00445-019-1268-y

Patrick, M., Wilson, D., Fee, D., Orr, T., Swanson, D., Sutton, A., & Elias, T. (2008). Gas-Pistoning associated with the 2008 summit eruption of Kilauea Volcano, Hawai'i. *AGU Fall Meeting Abstracts*, *2008*, V51E–2082.

Patrick, M., Wilson, D., Fee, D., Orr, T., & Swanson, D. (2011b). Shallow degassing events as a trigger for very-long-period seismicity at Kīlauea Volcano, Hawai'i. *Bulletin of Volcanology*, *73*(9), 1179–1186. https://doi.org/10.1007/s00445-011-0475-y

Pedersen, G. B., Belart, J. M., Óskarsson, B. V., Gudmundsson, M. T., Gies, N., Högnadóttir, T., et al. (2022b). Volume, effusion rate, and Lava transport during the 2021 fagradalsfjall eruption: Results from near real–time photogrammetric monitoring. *Geophysical Research Letters*, *49*(13), e2021GL097125. https://doi.org/10.1029/2021GL097125

Pedersen, G. B., Belart, J. M., Óskarsson, B. V., Gudmundsson, M. T., Gies, N., Högnadóttir, T., et al. (2022a). Digital elevation models, orthoimages and lava outlines of the 2021 Fagradalsfjall eruption: Results from near real-time photogrammetric monitoring. *Zenodo*. https://doi.org/10.5281/ZENODO.7866738

Rasband, W. S. (2012). *Image J: Image processing and analysis in Java*. Astrophysics Source Code Library, ascl:1206.013.

Reiss, M. C., Massimetti, F., Laizer, A. S., Campus, A., Rümpker, G., & Kazimoto, E. O. (2023). Overview of seismo-acoustic tremor at Oldoinyo Lengai, Tanzania: Shallow storage and eruptions of carbonatite melt. *Journal of Volcanology and Geothermal Research*, *442*, 107898. https://doi.org/10.1016/j.jvolgeores.2023.107898

Richardson, J. P., Waite, G. P., & Palma, J. L. (2014). Varying seismic–acoustic properties of the fluctuating lava Lake at Villarrica Volcano, Chile. *Journal of Geophysical Research: Solid Earth*, *119*(7), 5560–5573. https://doi.org/10.1002/2014JB011002

Ripepe, M., Delle Donne, D., Lacanna, G., Marchetti, E., & Ulivieri, G. (2009). The onset of the 2007 stromboli effusive eruption recorded by an integrated geophysical network. *Journal of Volcanology and Geothermal Research*, *182*(3–4), 131–136. https://doi.org/10.1016/j.jvolgeores.2009.02.011

Ripepe, M., & Gordeev, E. (1999). Gas bubble dynamics model for shallow volcanic tremor at stromboli. *Journal of Geophysical Research*, *104*(B5), 10639–10654. https://doi.org/10.1029/98JB02734

Sæmundsson, K., & Einarsson, P. (2014). Notes on the tectonics of Reykjanes. Iceland GeoSurvey, Report ÍSOR-2014 (Vol. *3*).

Sæmundsson, K., Sigurgeirsson, M. Á., & Friðleifsson, G. Ó. (2020). Geology and structure of the Reykjanes volcanic system, Iceland. *Journal of Volcanology and Geothermal Research*, *391*, 106501. https://doi.org/10.1016/j.jvolgeores.2018.11.022

Sigmundsson, F., Einarsson, P., Hjartardóttir, Á. R., Drouin, V., Jónsdóttir, K., Árnadóttir, T., et al. (2020). Geodynamics of Iceland and the signatures of plate spreading. *Journal of Volcanology and Geothermal Research*, *391*, 106436. https://doi.org/10.1016/j.jvolgeores.2018.08.014

Sigmundsson, F., Parks, M., Hooper, A., Geirsson, H., Vogfjörd, K. S., Drouin, V., et al. (2022). Deformation and seismicity decline before the 2021 Fagradalsfjall eruption. *Nature*, *609*(7927), 523–528. https://doi.org/10.1038/s41586-022-05083-4

Sigurdsson, H., Houghton, B. F., McNutt, S. R., Rymer, H., & Stix, J. (Eds.) (2015). *The encyclopedia of volcanoes* (2nd ed. ed.). Academic Press. Retrieved from https://oro.open.ac.uk/45054/

Smets, B., d'Oreye, N., Kervyn, M., & Kervyn, F. (2017). Gas piston activity of the Nyiragongo lava Lake: First insights from a stereographic time-lapse camera system. *Journal of African Earth Sciences*, *134*, 874–887. https://doi.org/10.1016/j.jafrearsci.2016.04.010

Swanson, D. A., Duffield, W. A., Jackson, D. B., & Peterson, D. W. (1979). *Chronological narrative of the 1969–71 Mauna Ulu eruption of Kilauea volcano*. Professional Paper (1056). https://doi.org/10.3133/pp1056

Tazieff, H. (1994). Permanent lava Lakes: Observed facts and induced mechanisms. *Journal of Volcanology and Geothermal Research*, *63*(1–2), 3–11. https://doi.org/10.1016/0377-0273(94)90015-9

Valade, S., Ripepe, M., Giuffrida, G., Karume, K., & Tedesco, D. (2018). Dynamics of Mount Nyiragongo lava Lake inferred from thermal imaging and infrasound array. *Earth and Planetary Science Letters*, *500*, 192–204. https://doi.org/10.1016/j.epsl.2018.08.004

Westoby, M. J., Brasington, J., Glasser, N. F., Hambrey, M. J., & Reynolds, J. M. (2012). Structure-from-Motion' photogrammetry: A low-cost, effective tool for geoscience applications. *Geomorphology*, *179*, 300–314. https://doi.org/10.1016/j.geomorph.2012.08.021

Witham, F., Woods, A. W., & Gladstone, C. (2006). An analogue experimental model of depth fluctuations in lava Lakes. *Bulletin of Volcanology*, *69*(1), 51–56. https://doi.org/10.1007/s00445-006-0055-8

Witter, J. B., & Harris, A. J. L. (2007). Field measurements of heat loss from skylights and lava tube systems. *Journal of Geophysical Research*, *112*(B1). https://doi.org/10.1029/2005JB003800

Zali, Z., Mousavi, S. M., Ohrnberger, M., Eibl, E. P. S., & cotton, f. (2024). Tremor clustering reveals pre-eruptive signals and evolution of the 2021 Geldingadalir eruption of the Fagradalsfjall fires, Iceland. *Communications Earth and Environment*, *5*(1), 1–11. https://doi.org/10.1038/s43247-023-01166-w